<div align="center">

Supporting Information

Controlling the symmetry of hexamonodentate 3d-transition metal complexes through symmetry propagation from high-symmetry Ti–Mo and Zr–Mo clusters via hydrogen-bonding interactions

</div>

<div align="center">

Ryoji Mitsuhashi,[1,*] Yuya Imai,[2] Sugiarto,[2] Hiroshi Sakiyama,[3] Yuji Kikukawa,[2] Yoshihito Hayashi[2*]

[1] Institute of Liberal Arts and Science, Kanazawa University; Kakuma, Kanazawa, Ishikawa 920-1192, Japan
[2] Department of Chemistry, Kanazawa University; Kakuma, Kanazawa, Ishikawa 920-1192, Japan
[3] Department of Science, Faculty of Science, Yamagata University, 1-4-12 Kojirakawa, Yamagata, 990-8560, Japan

E-mail mitsuhashi@staff.kanazawa-u.ac.jp

</div>

Contents:

1. ^{1}H NMR spectrum

Figure S1. ^{1}H NMR spectra of **ZnZr** in dmso-d$_6$. Two sets of resonance peaks for N–H atoms were observed at 7.07 and 5.23 ppm in 1:2 integration ratio.

2. X-Ray crystallography

Table S1. Crystallographic information of **FeTi** and **FeZr**.
Table S2. Crystallographic information of **CoTi** and **CoZr**.
Table S3. Crystallographic information of **NiTi** and **NiZr**.
Table S4. Crystallographic information of **ZnTi** and **ZnZr**.
Figure S2. Crystal structures of the cationic part of **MTi** along the *a*-axis. (a) **FeTi**, (b) **CoTi**, (c) **NiTi** and (d) **ZnTi**. The perchlorate anions were removed for clarity. White and light blue balls are Ti and Mo, respectively.
Figure S3. Crystal structures of **MZr** along the *a*-axis. (a) **FeZr**, (b) **CoZr**, (c) **NiZr** and (d) **ZnZr**.The perchlorate anions were removed for clarity. Yellow and light blue balls are Zr and Mo, respectively.
Table S5. Selected distances and angles in **TiMo6^{4+}**.
Table S6. Selected bonding parameters in **ZrMo6^{4+}**.
Table S7. Selected bonding parameters around $[M(H_2O)_6]^{2+}$ cations (M = Fe, Co, Ni, and Zn; Å, °).
Figure S4. X-band powder EPR spectrum of **CoZr** at 4 K. The fitted parameter: g_x, g_y = 1.940, g_z = 8.450, Ax, Ay = 637 MHz, Az = 850 MHz.

3. EPR Measurements

Figure S4. X-band powder EPR spectrum of **CoZr** at 4 K. The fitted parameter: g_x, g_y = 1.940, g_z = 8.450, Ax, Ay = 637 MHz, Az = 850 MHz.

4. Magnetic Measurements

Figure S5. Magnetization curves for (a) **FeTi** , (b) **CoTi** and, (c) **NiTi** at 2, 4, 6, and 8 K. The black solid lines represent fits of the Hamiltonians.
Figure S6. Magnetization curves for (a) **FeZr**, (b) **CoZr** and, (c) **NiZr** at 2, 4, 6, and 8 K. The black solid lines represent fits of the Hamiltonians.
Figure S7. Dc field dependence of (a) the χ_M' vs. frequency plots and (b) χ_M'' vs. frequency plots for **CoTi** at 1.9 K with ac frequency of 1–1488 Hz. The lines are guide for the eye.
Figure S8. (a) Cole–Cole plot for **CoTi** at 1.9 K under variable field. The solid lines represent the fit to a generalized Debye model. (b) The field dependence of the relaxation time derived from the fit.
Table S8. Cole-Cole fit values for **CoTi** at 1.9 K with an applied dc field of 0.2–4 kOe.
Figure S9. Temperature dependence of (a) the in-phase χ_M' vs. frequency plots and (b) out-of-phase χ_M'' vs. frequency plots for **CoTi** in the presence of 1 kOe with ac frequency of 1–1488 Hz. The lines are guide for the eye.

Figure S10. Cole–Cole plot for **CoTi** in the presence of 1 kOe dc field at variable temperature. The solid lines represent the fit to a generalized Debye model.

Table S9. Cole-Cole fit values for **CoTi** at 1.9–4.5 K with an applied dc field of 1 kOe.

Figure S11. Dc field dependence of (a) the in-phase χ_M' vs. frequency plots and (b) out-of-phase χ_M'' vs. frequency plots for **CoZr** at 1.9 K with ac frequency of 1–1488 Hz. The lines are guide for the eye.

Figure S12. (a) Cole–Cole plot for **CoZr** at 1.9 K under variable field. The solid lines represent the fit to a generalized Debye model. (b) The field dependence of the relaxation time derived from the fit.

Table S10. Cole-Cole fit values for **CoZr** at 1.9 K with an applied dc field of 0.2–5 kOe.

Figure S13. Temperature dependence of (a) the in-phase χ_M' vs. frequency plots and (b) out-of-phase χ_M'' vs. frequency plots for **CoZr** in the presence of 0.8 kOe with ac frequency of 1–1488 Hz. The lines are guide for the eye.

Figure S14. Cole–Cole plot for **CoZr** in the presence of 1 kOe dc field at variable temperature. The solid lines represent the fit to a generalized Debye model.

Table S11. Cole-Cole fit values for **CoZr** at 1.9–4.5 K with an applied dc field of 0.8 kOe.

Figure S15. The energy levels of d-orbital-related molecular orbitals for $[Ni(H_2O)_6]^{2+}$ complex cation in **NiTi** on the basis of the DFT computation (LC-BOP/6-31G).

Figure S16. The energy level diagrams for six-coordinate d^6 ion. (a) Bailar twisting distortion from. (b) Trigonal elongation/compression. Racah and AOM parameters: $B = 1050$ cm^{-1}, $C = 4500$ cm^{-1}, $e_\sigma = 4000$ cm^{-1}.

1. ^{1}H NMR spectrum
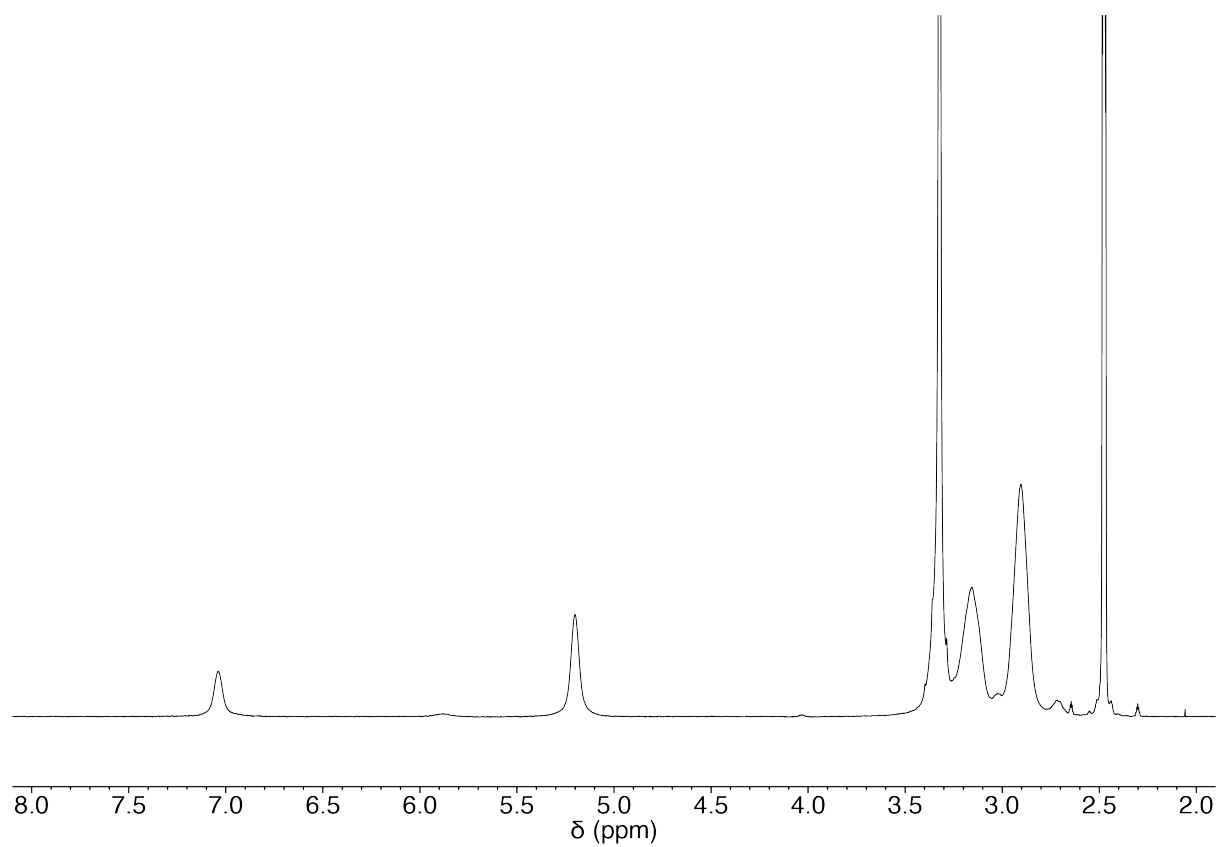
Figure S1. ^{1}H NMR spectra of **ZnZr** in dmso-d$_6$. Two sets of resonance peaks for N–H atoms were observed at 7.07 and 5.23 ppm in 1:2 integration ratio.

2. X-Ray crystallography

Table S1. Crystallographic information of **FeTi** and **FeZr**.

	FeTi	FeZr
Formula	$C_{36}H_{102}Cl_6FeMo_6N_{18}O_{48}Ti$	$C_{36}H_{102}Cl_6FeMo_6N_{18}O_{48}Zr$
Formula weight	2447.44	2490.76
Crystal system	Trigonal	Trigonal
Size / mm	0.14×0.12×0.09	0.10×0.06×0.04
Space group	$R3$	$R3$
a / Å	21.6648(4)	21.8319(4)
c / Å	14.6787(4)	14.7616(3)
V / Å^3	5966.6(3)	6093.2(3)
Z	3	3
T / K	104(2)	102(2)
Density / g cm^{-3}	2.043	2.036
μ / mm^{-1}	1.499	1.498
$F(000)$	3690	3744
$2\theta_{max}$ / °	55	55
No. of reflections measured	10783	10009
No. of independent reflections	4493 (R_{int} = 0.0210)	5470 (R_{int} = 0.0279)
Data/restraints/parameters	4493/148/399	5470/152/399
R_1 [I>2.00σ(I)]]	0.0317	0.0308
wR_2(all reflections)	0.0877	0.0790
Goodness of fit	0.822	1.075
Highest peak, deepest hole / e Å^{-3}	1.602, −1.700	0.745, −1.606
Flack	0.44(5)	0.019(18)
CCCDC Deposition #	2372554	2372558

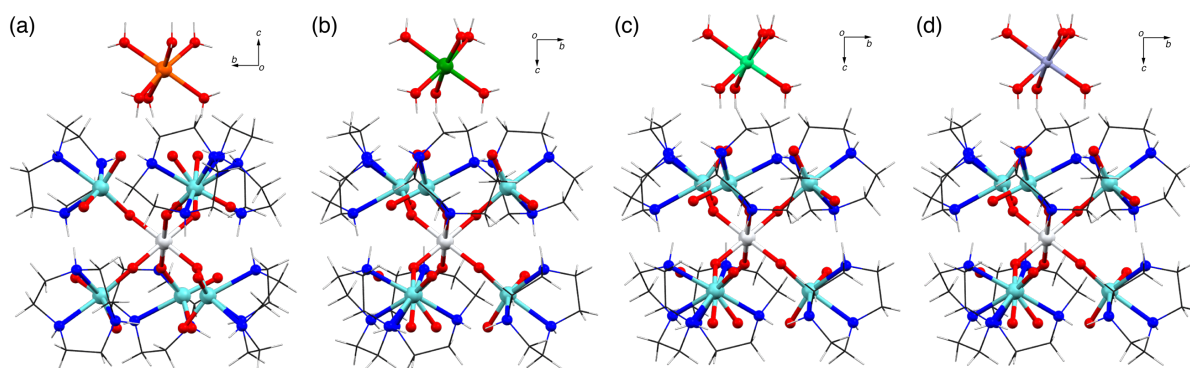**Table S2.** Crystallographic information of **CoTi** and **CoZr**.

	CoTi	CoZr
Formula	$C_{36}H_{102}Cl_6CoMo_6N_{18}O_{48}Ti$	$C_{36}H_{102}Cl_6CoMo_6N_{18}O_{48}Zr$
Formula weight	2450.52	2493.84
Crystal system	Trigonal	Trigonal
Size / mm	0.14×0.09×0.05	0.08×0.06×0.04
Space group	$R3$	$R3$
a / Å	21.5929(7)	21.7971(4)
c / Å	14.6575(5)	14.7552(3)
V / Å^3	5918.5(4)	6071.2(3)
Z	3	3
T / K	104(2)	102(2)
Density / g cm^{-3}	2.063	2.046
μ / mm^{-1}	1.537	1.529
$F(000)$	3693	3747
$2\theta_{max}$ / °	55	57
No. of reflections measured	9959	17067
No. of independent reflections	4799 (R_{int} = 0.0339)	6463 (R_{int} = 0.0296)
Data/restraints/parameters	4799/164/399	6463/252/411
R_1 [I>2.00σ(I)]]	0.0410	0.0354
wR_2(all reflections)	0.01091	0.0902
Goodness of fit	1.040	1.074
Highest peak, deepest hole / e Å^{-3}	1.022, −1.449	0.628, −1.739
Flack	0.44(5)	0.004(15)
CCCDC Deposition #	2372555	2372559

**Table S3.** Crystallographic information of **NiTi** and **NiZr**.

	NiTi	NiZr
Formula	$C_{36}H_{102}Cl_6Mo_6N_{18}NiO_{48}Ti$	$C_{36}H_{102}Cl_6Mo_6N_{18}NiO_{48}Zr$
Formula weight	2450.30	2493.62
Crystal system	Trigonal	Trigonal
Size / mm	0.16×0.12×0.06	0.08×0.07×0.04
Space group	$R3$	$R3$
a / Å	21.6510(8)	21.7869(4)
c / Å	14.6425(4)	14.6803(3)
V / Å^3	5944.3(5)	6034.7(3)
Z	3	3
T / K	100(2)	102(2)
Density / g cm^{-3}	2.053	2.058
μ / mm^{-1}	1.559	1.566
$F(000)$	3696	3750
$2\theta_{max}$ / °	55	55
No. of reflections measured	10374	8842
No. of independent reflections	4240 (R_{int} = 0.0346)	5351 (R_{int} = 0.0194)
Data/restraints/parameters	4240/148/399	6351/202/401
R_1 [I>2.00σ(I)]]	0.0428	0.0337
wR_2(all reflections)	0.01174	0.0902
Goodness of fit	0.984	1.074
Highest peak, deepest hole / e Å^{-3}	2.483, −1.447	0.759, −2.051
Flack	0.06(4)	0.00(4)
CCCDC Deposition #	2372556	2372560

Table S4. Crystallographic information of **ZnTi** and **ZnZr**.

	ZnTi	ZnZr
Formula	$C_{36}H_{102}Cl_6Mo_6N_{18}O_{48}TiZn$	$C_{36}H_{102}Cl_6Mo_6N_{18}O_{48}ZnZr$
Formula weight	2456.96	2500.28
Crystal system	Trigonal	Trigonal
Size / mm	0.22×0.16×0.12	0.16×0.11×0.06
Space group	$R3$	$R3$
a / Å	21.6448(3)	21.7780(3)
c / Å	14.6822(3)	14.7532(2)
V / Å^3	5957.0(3)	6059.72(19)
Z	3	3
T / K	104(2)	102(2)
Density / g cm^{-3}	2.055	2.055
μ / mm^{-1}	1.621	1.623
$F(000)$	3702	3756
$2\theta_{max}$ / °	55	55
No. of reflections measured	10464	10949
No. of independent reflections	4770 (R_{int} = 0.0123)	5055 (R_{int} = 0.0183)
Data/restraints/parameters	4799/170/399	5055/169/400
R_1 [I>2.00σ(I)]]	0.0292	0.0238
wR_2(all reflections)	0.00826	0.0640
Goodness of fit	1.040	1.083
Highest peak, deepest hole / e Å^{-3}	0.826, −2.077	0.533, −1.556
Flack	0.39(3)	0.15(2)
CCCDC Deposition #	2372557	2372561

Figure S2. Crystal structures of the cationic part of **MTi** along the *a*-axis. (a) **FeTi**, (b) **CoTi**, (c) **NiTi** and (d) **ZnTi**. The perchlorate anions were removed for clarity. White and light blue balls are Ti and Mo, respectively.
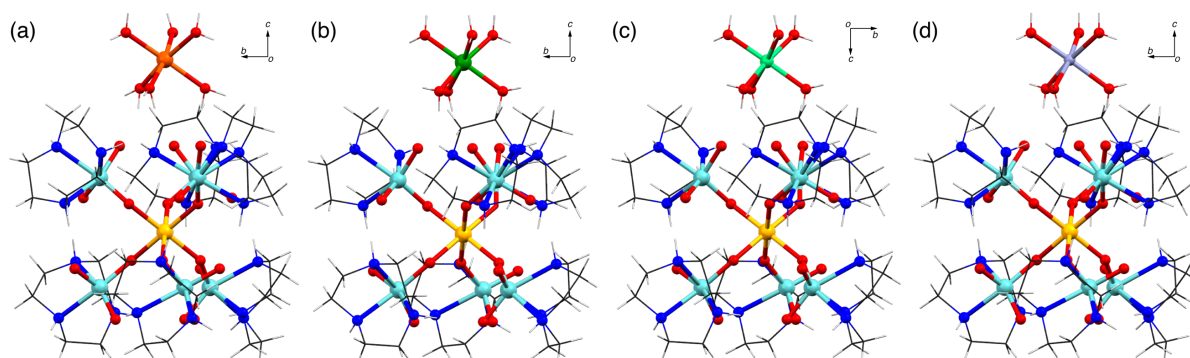
Figure S3. Crystal structures of **MZr** along the *a*-axis. (a) **FeZr**, (b) **CoZr**, (c) **NiZr** and (d) **ZnZr**. The perchlorate anions were removed for clarity. Yellow and light blue balls are Zr and Mo, respectively.

Table S5. Selected distances and angles in **MTi**.

	FeTi	**CoTi**	**NiTi**	**ZnTi**
Ti–O1 / Å	1.936(5)	1.937(6)	1.941(6)	1.937(4)
Ti–O4 / Å	1.936(4)	1.938(6)	1.935(6)	1.937(4)
O1-O1^i-O1^{ii}··· O4-O4^i-O4^{ii} / Å	2.232(7)	2.224(8)	2.228(8)	2.233(6)
Mo1···Mo2 / Å	4.601(1)	4.600(1)	4.612(1)	4.608(1)
Mo1···Mo1^i / Å	4.620(1)	4.619(1)	4.630(1)	4.625(1)
Mo2···Mo2^i / Å	4.726(1)	4.717(1)	4.714(1)	4.723(3)
Mo1-Mo1^i-Mo1^{ii}··· Mo2-Mo2^i-Mo2^{ii} / Å	4.554(1)	4.552(1)	4.562(1)	4.560(1)
Short Ti···M / Å	7.270(3)	7.243(4)	7.222(4)	7.257(3)
Long Ti···M / Å	7.408(3)	7.415(4)	7.421(4)	7.425(3)

Symmetry code: (*i* = '–x+y, 1–x, z', *ii* = '1-y, x–y+1, z').

Table S6. Selected bonding parameters in **MZr**.

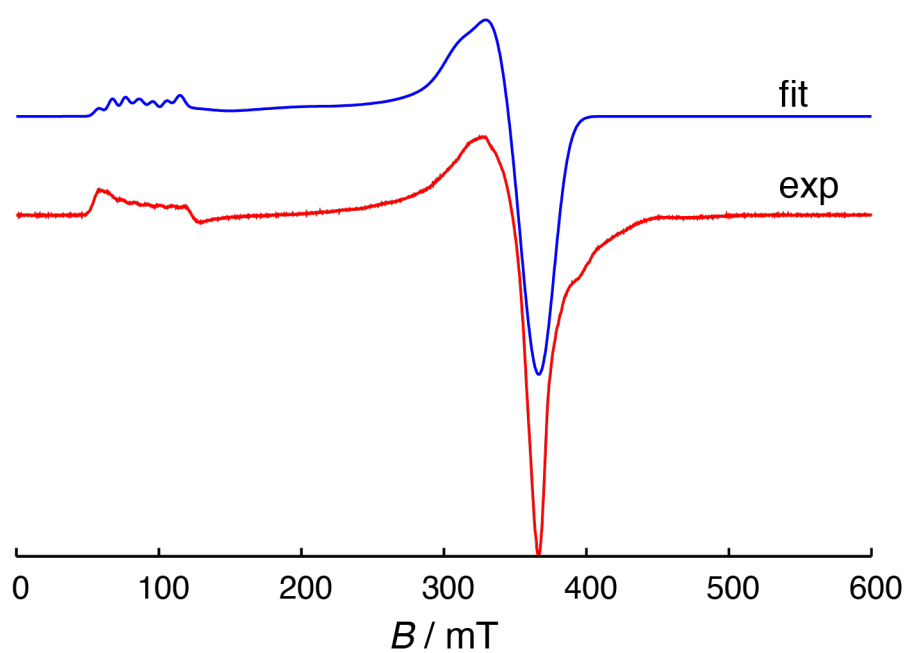|	**FeZr**	**CoZr**	**NiZr**	**ZnZr**
Zr–O1 / Å	2.072(4)	2.066(5)	2.066(5)	2.070(4)
Zr–O4 / Å	2.075(4)	2.078(5)	2.077(5)	2.068(4)
O1-O1^i-O1^{ii}··· O4-O4^i-O4^{ii} / Å	2.395(7)	2.401(6)	2.394(7)	2.594(5)
Mo1···Mo2 / Å	4.700(1)	4.702(1)	4.703(1)	4.702(1)
Mo1···Mo1^i / Å	4.795(1)	4.798(1)	4.795(1)	4.793(1)
Mo2···Mo2^i / Å	4.908(1)	4.904(1)	4.892(1)	4.890(3)
Mo1-Mo1^i-Mo1^{ii}··· Mo2-Mo2^i-Mo2^{ii} / Å	4.657(1)	4.658(1)	4.658(1)	4.656(1)
Short Zr···M / Å	7.307(3)	7.283(3)	7.226(3)	7.278(2)
Long Zr···M / Å	7.455(3)	7.472(3)	7.454(3)	7.475(2)

Symmetry code: (*i* = '–x+y, 1–x, z', *ii* = '1-y, x–y+1, z').

Table S7. Selected bonding parameters around $[M(H_2O)_6]^{2+}$ cations (M = Fe, Co, Ni, and Zn; Å, °).

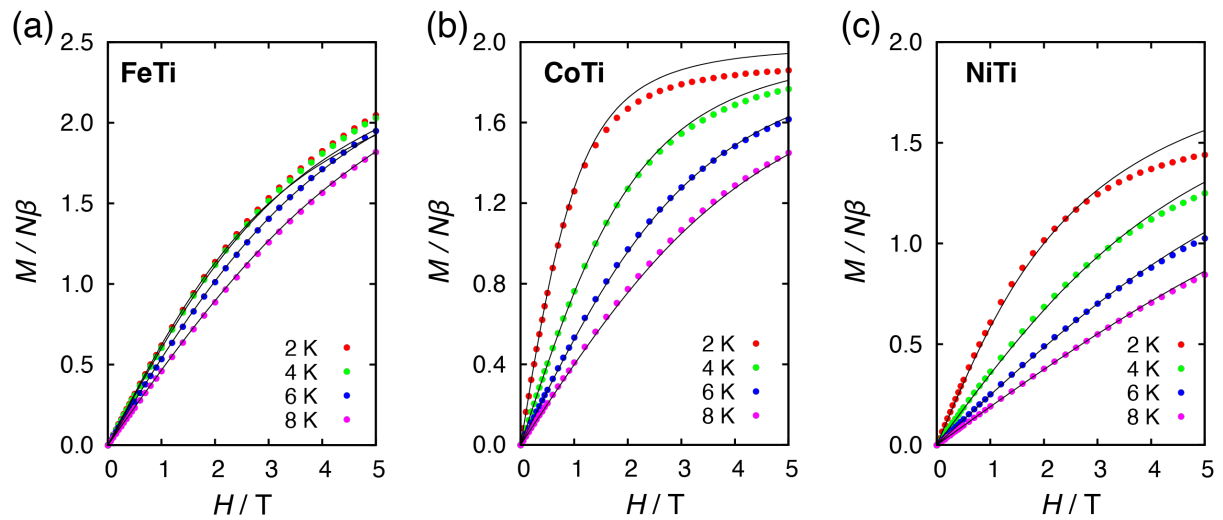|	FeTi	FeZr	CoTi	CoZr	NiTi	NiZr	ZnTi	ZnZr
M–O7	2.103(6)	2.114(6)	2.086(7)	2.082(6)	2.046(8)	2.037(7)	2.082(6)	2.084(4)
M–O8	2.089(6)	2.090(6)	2.062(8)	2.060(6)	2.017(8)	2.030(7)	2.044(6)	2.058(4)
O7⋯O7^i	2.974(10)	2.989(11)	2.913(14)	2.922(11)	2.875(14)	2.881(12)	2.915(11)	2.922(8)
O8⋯O8^i	3.037(12)	3.029(11)	2.967(16)	2.955(12)	2.918(15)	2.927(13)	2.952(12)	2.964(9)
s (average)	3.01	3.01	2.94	2.94	2.90	2.90	2.93	2.94
h	2.351(10)	2.365(9)	2.383(11)	2.376(9)	2.305(10)	2.301(10)	2.353(9)	2.367(7)
s/h	1.28	1.27	1.23	1.24	1.26	1.26	1.25	1.24
φ	48.8(3)	48.8(4)	49.5(5)	49.7(4)	52.9(4)	52.8(5)	49.8(4)	49.7(3)

Symmetry code: (i = '–x+y, 1–x, +z').
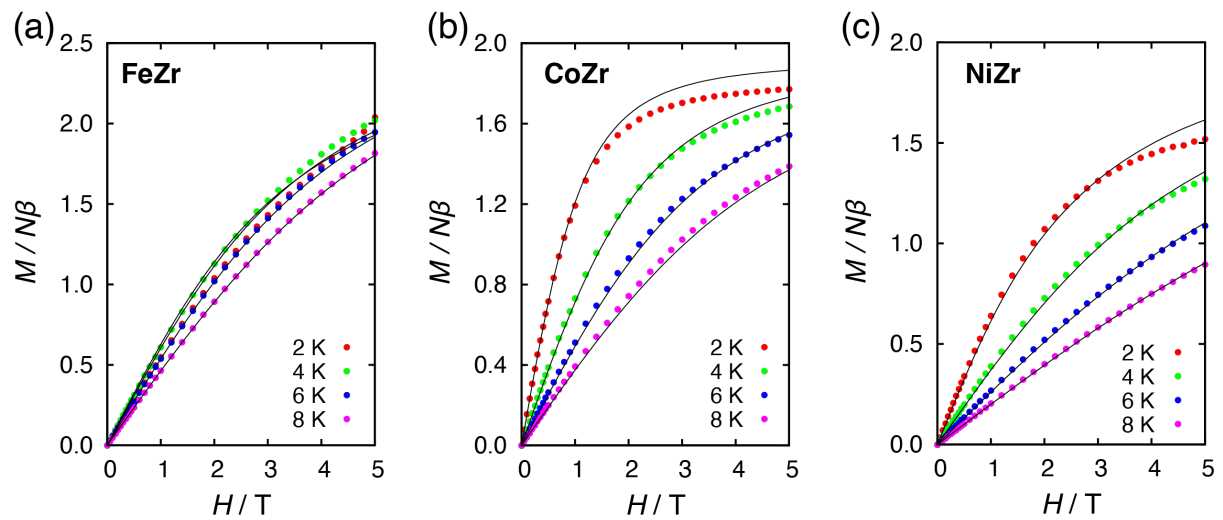
3. EPR Measurements

Figure S4. X-band powder EPR spectrum of **CoZr** at 4 K. The fitted parameter: g_x, g_y = 1.940, g_z = 8.450, Ax, Ay = 637 MHz, Az = 850 MHz.
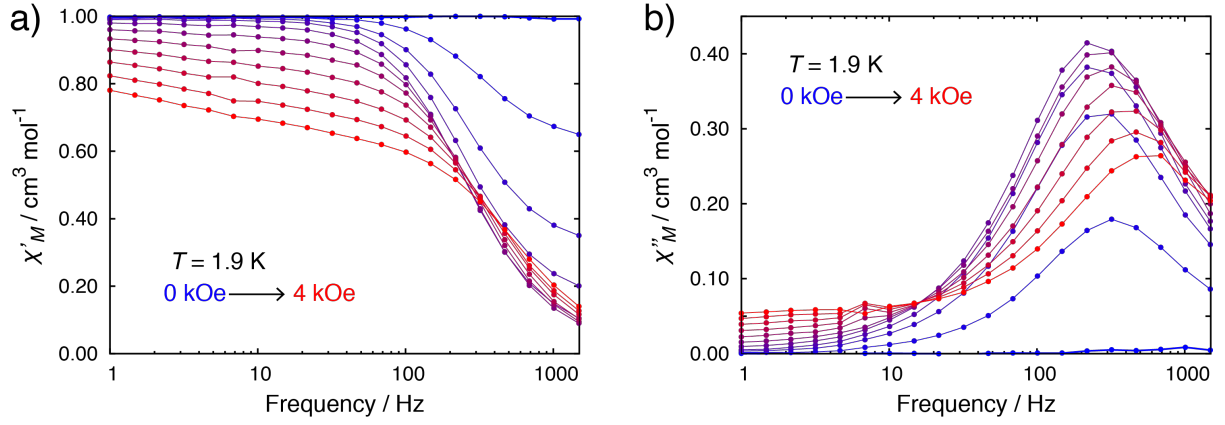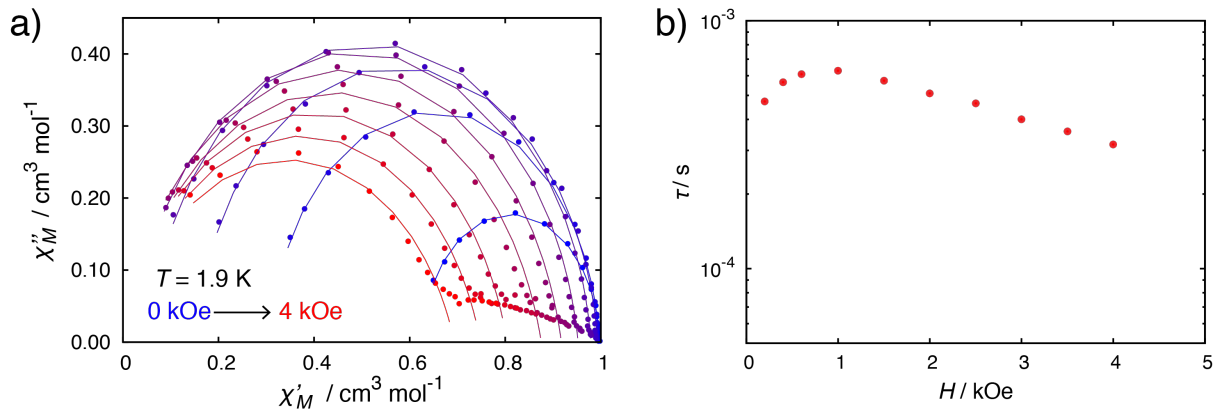
4. Magnetic Measurements

Figure S5. Magnetization curves for (a) **FeTi** , (b) **CoTi** and, (c) **NiTi** at 2, 4, 6, and 8 K. The black solid lines represent fits of the Hamiltonians.

Figure S6. Magnetization curves for (a) **FeZr**, (b) **CoZr** and, (c) **NiZr** at 2, 4, 6, and 8 K. The black solid lines represent fits of the Hamiltonians.
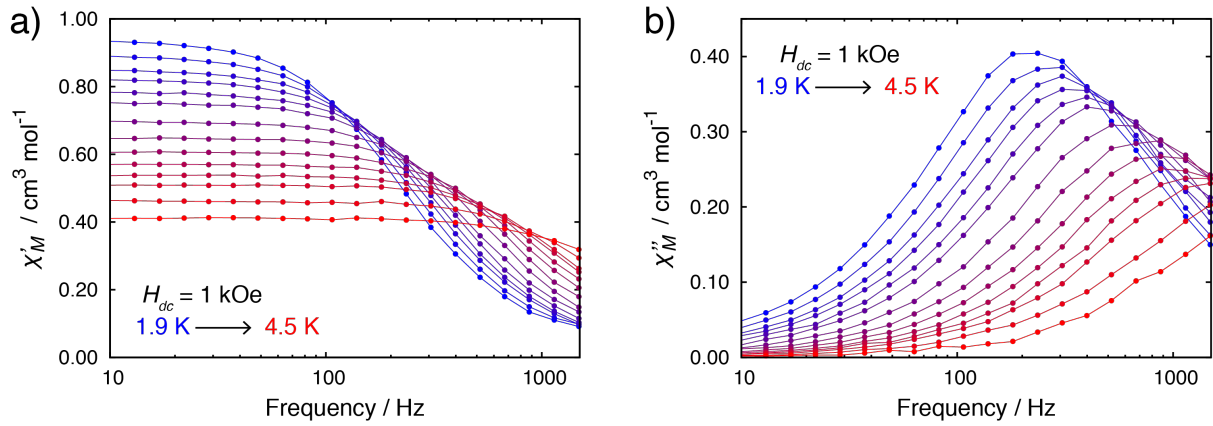
Figure S7. Dc field dependence of (a) the χ_M' vs. frequency plots and (b) χ_M'' vs. frequency plots for **CoTi** at 1.9 K with ac frequency of 1–1488 Hz. The lines are guide for the eye.
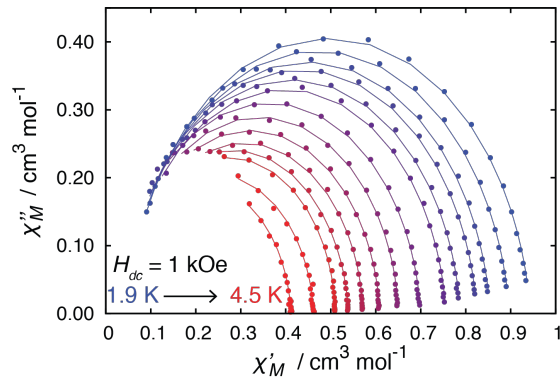

Figure S8. (a) Cole–Cole plot for **CoTi** at 1.9 K under variable field. The solid lines represent the fit to a generalized Debye model. (b) The field dependence of the relaxation time derived from the fit.

Table S8. Cole-Cole fit values for **CoTi** at 1.9 K with an applied dc field of 0.2–4 kOe.

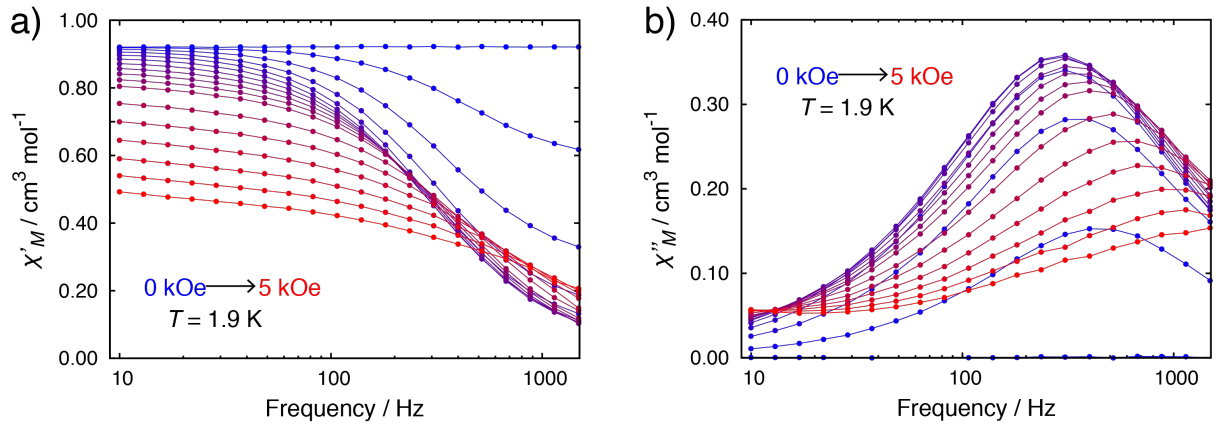| H / kOe	χ_S /cm$_3$ mol^{-1}	χ_T /cm$_3$ mol^{-1}	τ / s	α
0.2	6.274×10^{-1}	9.968×10^{-1}	4.722×10^{-4}	2.459×10^{-2}
0.4	3.088×10^{-1}	9.965×10^{-1}	5.655×10^{-4}	4.559×10^{-2}
0.6	1.528×10^{-1}	9.934×10^{-1}	6.094×10^{-4}	6.043×10^{-2}
1.0	5.484×10^{-2}	9.794×10^{-1}	6.280×10^{-4}	7.068×10^{-2}
1.5	1.949×10^{-2}	9.526×10^{-1}	5.725×10^{-4}	9.316×10^{-2}
2.0	1.034×10^{-14}	9.174×10^{-1}	5.093×10^{-4}	1.233×10^{-1}
2.5	1.374×10^{-14}	8.755×10^{-1}	4.649×10^{-4}	1.477×10^{-1}
3.0	2.118×10^{-15}	8.038×10^{-1}	4.004×10^{-4}	1.485×10^{-1}
3.5	2.667×10^{-15}	7.478×10^{-1}	3.574×10^{-4}	1.685×10^{-1}
4.0	3.824×10^{-15}	6.937×10^{-1}	3.167×10^{-4}	1.982×10^{-1}

Figure S9. Temperature dependence of (a) the in-phase χ_M' vs. frequency plots and (b) out-of-phase χ_M'' vs. frequency plots for **CoTi** in the presence of 1 kOe with ac frequency of 1–1488 Hz. The lines are guide for the eye.
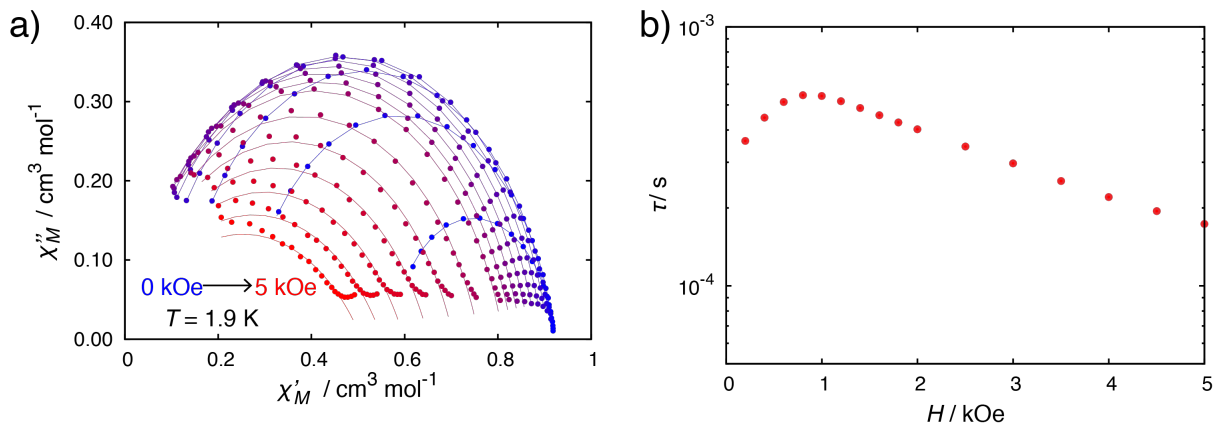

Figure S10. Cole–Cole plot for **CoTi** in the presence of 1 kOe dc field at variable temperature. The solid lines represent the fit to a generalized Debye model.

Table S9. Cole-Cole fit values for **CoTi** at 1.9–4.5 K with an applied dc field of 1 kOe.

| T / K	χ_S/cm$_3$ mol^{-1}	χ_T/cm$_3$ mol^{-1}	τ / s	α
1.9	4.828×10^{-2}	9.438×10^{-1}	6.900×10^{-4}	6.342×10^{-2}
2.0	4.459×10^{-2}	8.971×10^{-1}	5.873×10^{-4}	6.193×10^{-2}
2.1	4.056×10^{-2}	8.550×10^{-1}	5.009×10^{-4}	6.048×10^{-2}
2.2	3.983×10^{-2}	8.250×10^{-1}	4.496×10^{-4}	5.715×10^{-2}
2.3	3.717×10^{-2}	7.881×10^{-1}	3.879×10^{-4}	5.520×10^{-2}
2.4	4.246×10^{-2}	7.559×10^{-1}	3.432×10^{-4}	4.959×10^{-2}
2.6	2.766×10^{-2}	6.997×10^{-1}	2.653×10^{-4}	5.100×10^{-2}
2.8	3.454×10^{-2}	6.509×10^{-1}	2.183×10^{-4}	4.012×10^{-2}
3.0	3.431×10^{-2}	6.089×10^{-1}	1.804×10^{-4}	4.049×10^{-2}
3.2	4.249×10^{-2}	5.721×10^{-1}	1.546×10^{-4}	3.328×10^{-2}
3.4	2.518×10^{-2}	5.395×10^{-1}	1.256×10^{-4}	4.201×10^{-2}
3.6	3.337×10^{-2}	5.103×10^{-1}	1.124×10^{-4}	2.255×10^{-2}
4.0	2.478×10^{-2}	4.618×10^{-1}	8.194×10^{-5}	4.197×10^{-2}
4.5	5.065×10^{-3}	4.112×10^{-1}	5.605×10^{-5}	3.674×10^{-2}

Figure S11. Dc field dependence of (a) the in-phase χ_M' vs. frequency plots and (b) out-of-phase χ_M'' vs. frequency plots for **CoZr** at 1.9 K with ac frequency of 1–1488 Hz. The lines are guide for the eye.
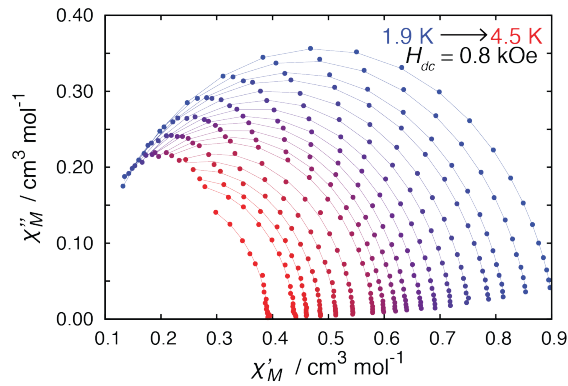

Figure S12. (a) Cole–Cole plot for **CoZr** at 1.9 K under variable field. The solid lines represent the fit to a generalized Debye model. (b) The field dependence of the relaxation time derived from the fit.

Table S10. Cole-Cole fit values for **CoZr** at 1.9 K with an applied dc field of 0.2–5 kOe.

H / kOe	χ_S/cm^3 mol^{-1}	χ_T/cm^3 mol^{-1}	τ / s	α
0.2	5.756×10^{-1}	9.205×10^{-1}	3.634×10^{-4}	7.601×10^{-2}
0.4	2.568×10^{-1}	9.206×10^{-1}	4.461×10^{-4}	1.020×10^{-1}
0.6	1.126×10^{-1}	9.155×10^{-1}	5.130×10^{-4}	1.070×10^{-1}
0.8	5.894×10^{-2}	9.074×10^{-1}	5.448×10^{-4}	1.110×10^{-1}
1.0	3.265×10^{-2}	8.968×10^{-1}	5.410×10^{-4}	1.209×10^{-1}
1.2	1.735×10^{-2}	8.829×10^{-1}	5.171×10^{-4}	1.307×10^{-1}
1.4	6.783×10^{-3}	8.675×10^{-1}	4.856×10^{-4}	1.402×10^{-1}
1.6	7.289×10^{-8}	8.505×10^{-1}	4.556×10^{-4}	1.480×10^{-1}
1.8	1.066×10^{-7}	8.320×10^{-1}	4.283×10^{-4}	1.553×10^{-1}
2.0	1.465×10^{-7}	8.117×10^{-1}	4.025×10^{-4}	1.621×10^{-1}
2.5	2.226×10^{-7}	7.598×10^{-1}	3.450×10^{-4}	1.880×10^{-1}
3.0	3.137×10^{-7}	7.050×10^{-1}	2.975×10^{-4}	2.164×10^{-1}
3.5	3.506×10^{-7}	6.516×10^{-1}	2.539×10^{-4}	2.542×10^{-1}
4.0	4.876×10^{-7}	5.992×10^{-1}	2.203×10^{-4}	2.933×10^{-1}
4.5	4.839×10^{-7}	5.523×10^{-1}	1.942×10^{-4}	3.422×10^{-1}
5.0	5.542×10^{-7}	5.083×10^{-1}	1.736×10^{-4}	3.881×10^{-1}
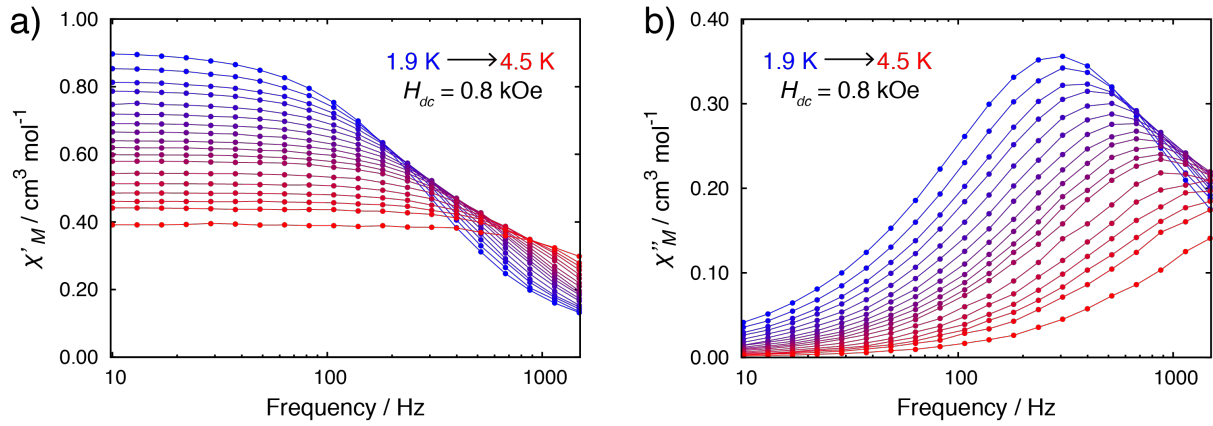
Figure S13. Temperature dependence of (a) the in-phase $\chi_M{'}$ vs. frequency plots and (b) out-of-phase $\chi_M{''}$ vs. frequency plots for **CoZr** in the presence of 0.8 kOe with ac frequency of 1–1488 Hz. The lines are guide for the eye.

Figure S14. Cole–Cole plot for **CoZr** in the presence of 1 kOe dc field at variable temperature. The solid lines represent the fit to a generalized Debye model.

Table S11. Cole-Cole fit values for **CoZr** at 1.9–4.5 K with an applied dc field of 0.8 kOe.

T / K	χ_S/cm$_3$ mol^{-1}	χ_T/cm$_3$ mol^{-1}	τ / s	α
1.9	5.894×10^{-2}	9.074×10^{-1}	5.448×10^{-4}	1.110×10^{-1}
2.0	5.322×10^{-2}	8.627×10^{-1}	4.742×10^{-4}	1.101×10^{-1}
2.1	5.087×10^{-2}	8.215×10^{-1}	4.162×10^{-4}	1.083×10^{-1}
2.2	4.690×10^{-2}	7.931×10^{-1}	3.778×10^{-4}	1.079×10^{-1}
2.3	4.744×10^{-2}	7.555×10^{-1}	3.355×10^{-4}	1.032×10^{-1}
2.4	4.718×10^{-2}	7.246×10^{-1}	3.006×10^{-4}	1.024×10^{-1}
2.5	4.027×10^{-2}	6.964×10^{-1}	2.670×10^{-4}	1.062×10^{-1}
2.6	4.256×10^{-2}	6.698×10^{-1}	2.439×10^{-4}	1.017×10^{-1}
2.7	4.031×10^{-2}	6.440×10^{-1}	2.211×10^{-4}	9.659×10^{-2}
2.8	4.436×10^{-2}	6.229×10^{-1}	2.064×10^{-4}	9.403×10^{-2}
2.9	4.078×10^{-2}	6.024×10^{-1}	1.874×10^{-4}	9.853×10^{-2}
3.0	4.229×10^{-2}	5.830×10^{-1}	1.730×10^{-4}	9.504×10^{-2}
3.2	4.652×10^{-2}	5.469×10^{-1}	1.505×10^{-4}	8.741×10^{-2}
3.4	3.741×10^{-2}	5.155×10^{-1}	1.270×10^{-4}	8.761×10^{-2}
3.6	3.808×10^{-2}	4.877×10^{-1}	1.106×10^{-4}	8.300×10^{-2}
3.8	4.584×10^{-2}	4.626×10^{-1}	9.926×10^{-5}	7.598×10^{-2}
4.0	4.561×10^{-2}	4.408×10^{-1}	8.670×10^{-5}	6.919×10^{-2}

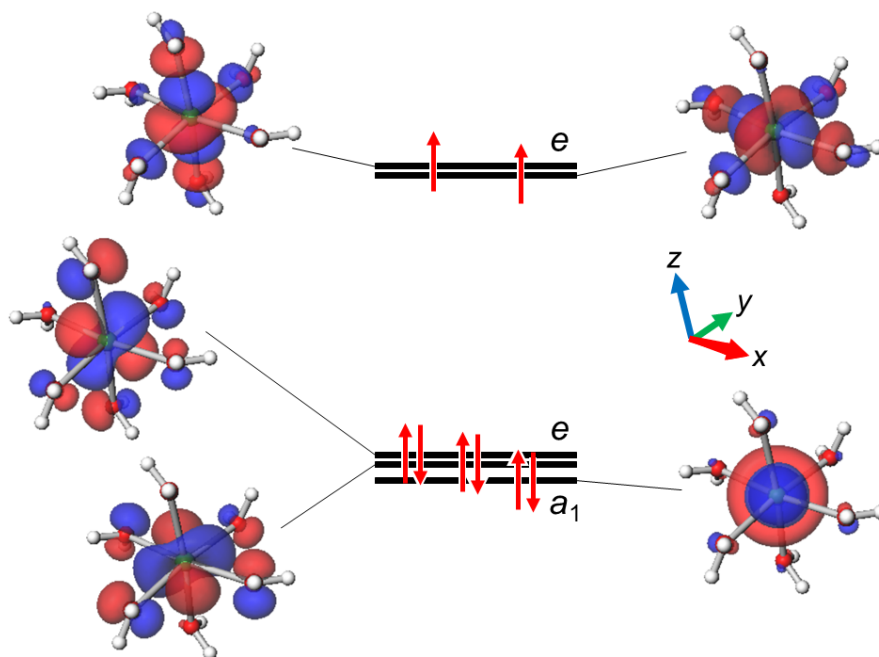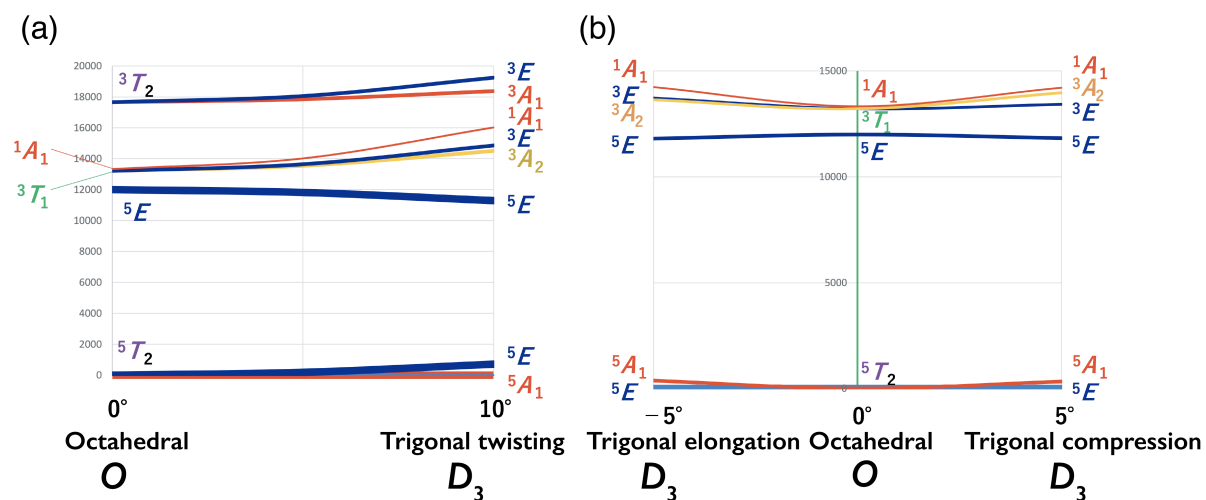| 4.5 | 4.007×10^{-2} | 3.926×10^{-1} | 6.043×10^{-5} | 5.809×10^{-2} |

4. DFT Calculation

Figure S15. The energy levels of d-orbital-related molecular orbitals for $[Ni(H_2O)_6]^{2+}$ complex cation in **NiTi** on the basis of the DFT computation (LC-BOP/6-31G).

4. AOM Calculation

Figure S16. The energy level diagrams for six-coordinate d^6 ion. (a) Bailar twisting distortion from. (b) Trigonal elongation/compression. Racah and AOM parameters: $B = 1050$ cm^{-1}, $C = 4500$ cm^{-1}, $e_\sigma = 4000$ cm^{-1}.